Electronic Supporting Information

Amplified Excited State Diverse Effects Arising from Ligand Regioisomerism in Cu(I) Complexes for Advanced Applications

Cecilia Bruschi,[1]† Dominik Graf,[2] Olaf Fuhr,[2,3] Valerio Cuboni,[4] Raffaella Lettieri,[4] Emanuela Gatto,[4] Sergei Lebedkin,[2] Angela Bihlmeier,[5] Claudia Bizzarri*[1,4]*

[1]Institute of Organic Chemistry (IOC), Karlsruhe Institute of Technology (KIT), Fritz-Haber-Weg 6, 76131 Karlsruhe, Germany
[2]Institute of Nanotechnology (INT), Karlsruhe Institute of Technology (KIT), Hermann-von-Helmholtz-Platz 1, 76344 Eggenstein-Leopoldshafen, Germany
[3]Karlsruhe Nano Micro Facility (KNMFi), Karlsruhe Institute of Technology (KIT), Hermann-von-Helmholtz-Platz 1, 76344 Eggenstein-Leopoldshafen, Germany
[4]Department of Chemical Sciences and Technologies, University of Rome Tor Vergata, via della Ricerca Scientifica, 00133 Rome, Italy
[5]Institute of Physical Chemistry (IPC), Karlsruhe Institute of Technology (KIT), Fritz-Haber-Weg 2, 76131 Karlsruhe, Germany

Table of Contents

1. Synthetic procedures

3-((triisopropylsilyl)ethynyl)quinoxalin-2(1*H*)-one (2). 1,2-Phenylendiamine (0. 440 g, 4.07 mmol, 1.00 equiv.) was reacted with methyl 2-oxo-4-(triisopropylsilyl)but-3-ynoate (**1**) (1.42 g, 5.29 mmol, 1.50 equiv.) into a 100 mL solution of ethanol and acetic acid (7:3) at 80°C for 15 h. After this time, the reaction mixture was quenched with water. The organic product was extracted three times with DCM. The combined organic phases were washed with water (three times), brine and then dried over Na_2SO_4 and filtered. The solvent was reduced under vacuum. The product was obtained without the need of a purification as a light-yellow powder. (1.14 g, 3.50 mmol) Yield: 86%. ^{1}H NMR (400 MHz, $CDCl_3$) δ = 12.91 (s, 1H, $H_{aromatic}$), 7.91 – 7.85 (m, 1H, $H_{aromatic}$), 7.52 (td, *J* = 7.8, 1.4 Hz, 1H, $H_{aromatic}$), 7.36 (t, *J* = 7.5 Hz, 2H, $H_{aromatic}$), 1.23 (m, *J* = 4.2 Hz, 21H, $H_{isopropyl}$) ppm. ^{13}C NMR (101 MHz, $CDCl_3$) δ = 156.54, 133.37, 131.39, 131.12, 129.56, 124.74, 115.99, 102.61, 101.97, 18.83, 11.46 ppm. HRMS (ESI) *m/z* ($C_{19}H_{26}N_2OSi$): 327.1892 (calc.), 327.1883 (found).

1-ethyl-3-((triisopropylsilyl)ethynyl)quinoxalin-2(1*H*)-one (3k) and 2-ethoxy-3-((triisopropylsilyl)ethynyl)quinoxaline (3e)

((Triisopropylsilyl)ethynyl)quinoxalin-2(1*H*)-one (**2**) (1.130 g, 3.46 mmol, 1.00 equiv.) and K_2CO_3 (1.190 g, 8.65 mmol, 2.50 equiv.) were dissolved in anhydrous DMF (5 mL). After 30 minutes, iodoethane (0.69 mL, 1.34 g, 8.65 mmol, 2.50 equiv.) was added and the reaction was left under stirring at 50°C for two hours. After this period time, water was added. The organic product was then extracted with DCM (three times), washed with water and brine, dried over Na_2SO_4 and filtered. The solvent was removed under vacuum. Two products were obtained **3k** and **3e** and purified by a silica gel column chromatography using Cyclohexane/DCM (30:70) as eluent. The main product (**3k**), bearing the ethyl group attached to the nitrogen atom, was obtained as a light-yellow solid with a yield of 54% (0.660 g, 1.86 mmol). ^{1}H NMR (400 MHz, $CDCl_3$) δ = 7.88 (dd, *J* = 8.1, 1.6 Hz, 1H, $H_{aromatic}$), 7.56 (ddd, *J* = 8.6, 7.3, 1.6 Hz, 1H, $H_{aromatic}$), 7.36 – 7.29 (m, 2H, $H_{aromatic}$), 4.33 (q, *J* = 7.2 Hz, 2H, C*H*$_2$), 1.39 (t, *J* = 7.2 Hz, 3H, C*H*$_3$), 1.23 – 1.17 (m, 21H, $H_{isopropyl}$) ppm. ^{13}C NMR (101 MHz, $CDCl_3$) δ = 154.08, 142.58, 133.61, 132.34, 131.33, 130.85, 123.84, 113.66, 102.53, 101.35, 37.81, 18.83, 12.51, 11.44 ppm. HRMS (ESI) *m/z* ([M+H]+, ($C_{21}H_30N_2OSi$)): 355.2206 (calc.), 355.2194 (found). The other regioisomer (**3e**), with the ethyl group linked to the oxygen atom, was isolated as a white solid with a yield of 27% (0.330 g, 0.93 mmol). ^{1}H NMR (400 MHz, $CDCl_3$) δ = 7.98 (dd, J = 8.2, 1.5 Hz, 1H, $H_{aromatic}$), 7.77 (dd, J = 8.4, 1.4 Hz, 1H, $H_{aromatic}$), 7.63 (ddd, J = 8.3, 7.0, 1.5 Hz, 1H, $H_{aromatic}$), 7.53 (ddd, J = 8.4, 7.0, 1.5 Hz, 1H, $H_{aromatic}$), 4.54 (q, J = 7.1 Hz, 2H, CH2), 1.48 (t, J = 7.1 Hz, 3H, CH_3), 1.19 (m, J = 3.8 Hz, 21H, $H_{isopropyl}$) ppm. ^{13}C NMR (101 MHz, $CDCl_3$) δ 157.59, 139.68, 138.52, 132.95, 130.51, 128.89, 126.94, 126.89, 101.71, 100.22, 63.08, 27.07, 18.82, 14.50, 11.43 ppm. HRMS (ESI) m/z ([M+H]+, ($C_{21}H_{30}N_2OSi$)): 355.2206 (calc.), 355.2194 (found).

2. NMR data

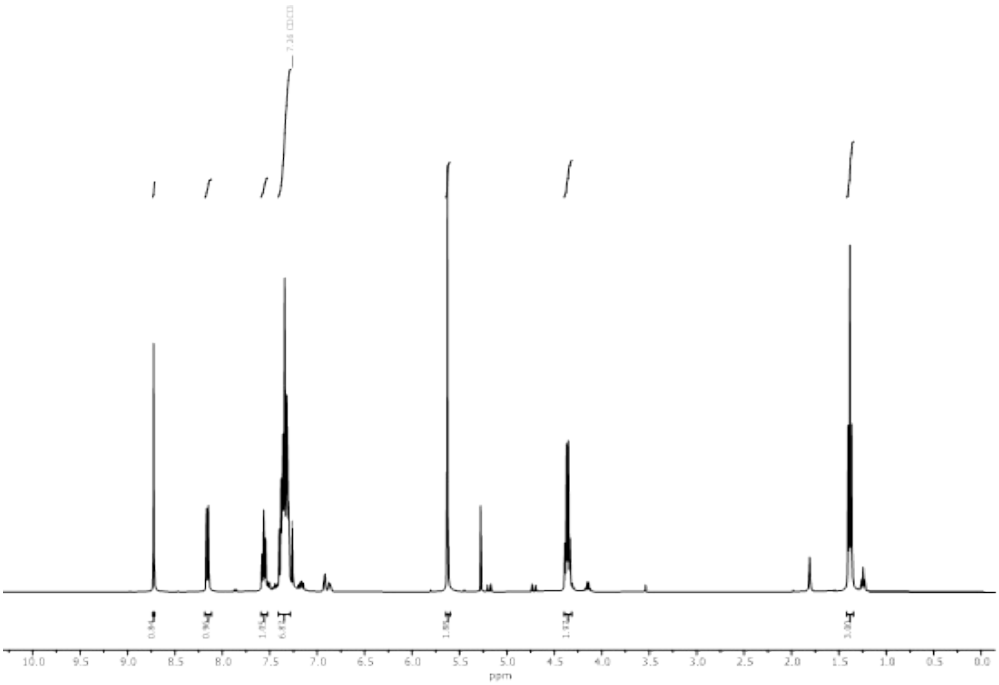

Figure S1. ^{1}H NMR (400 MHz, $CDCl_3$) of ligand **4k (**3-(1-benzyl-1H-1,2,3-triazol-4-yl)-1-ethylquinoxalin-2(1H)-one).

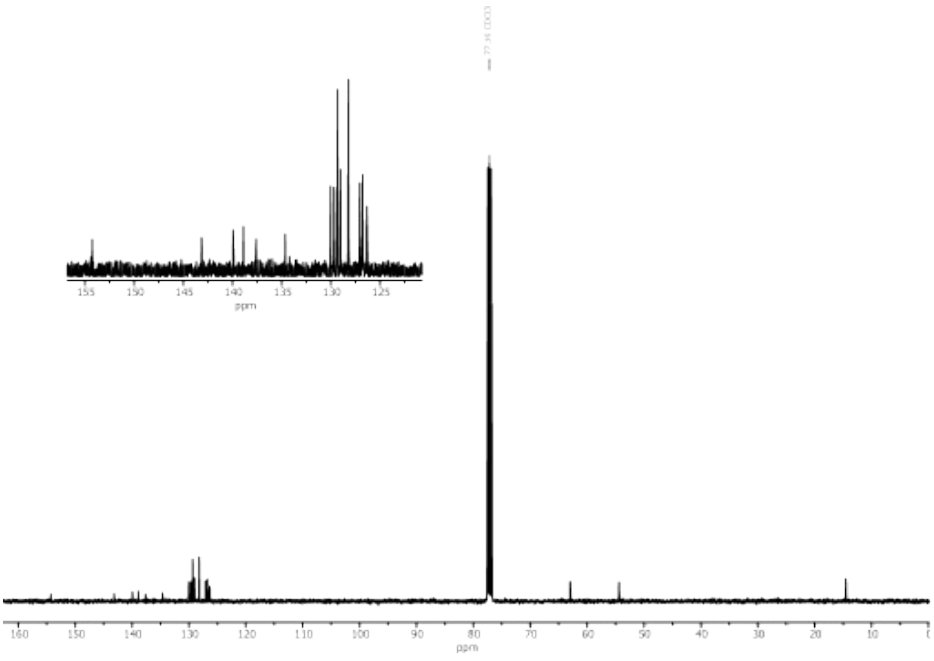

Figure S2. ^{13}C NMR (101 MHz, $CDCl_3$) of ligand **4k** (3-(1-benzyl-1H-1,2,3-triazol-4-yl)-1-ethylquinoxalin-2(1H)-one).

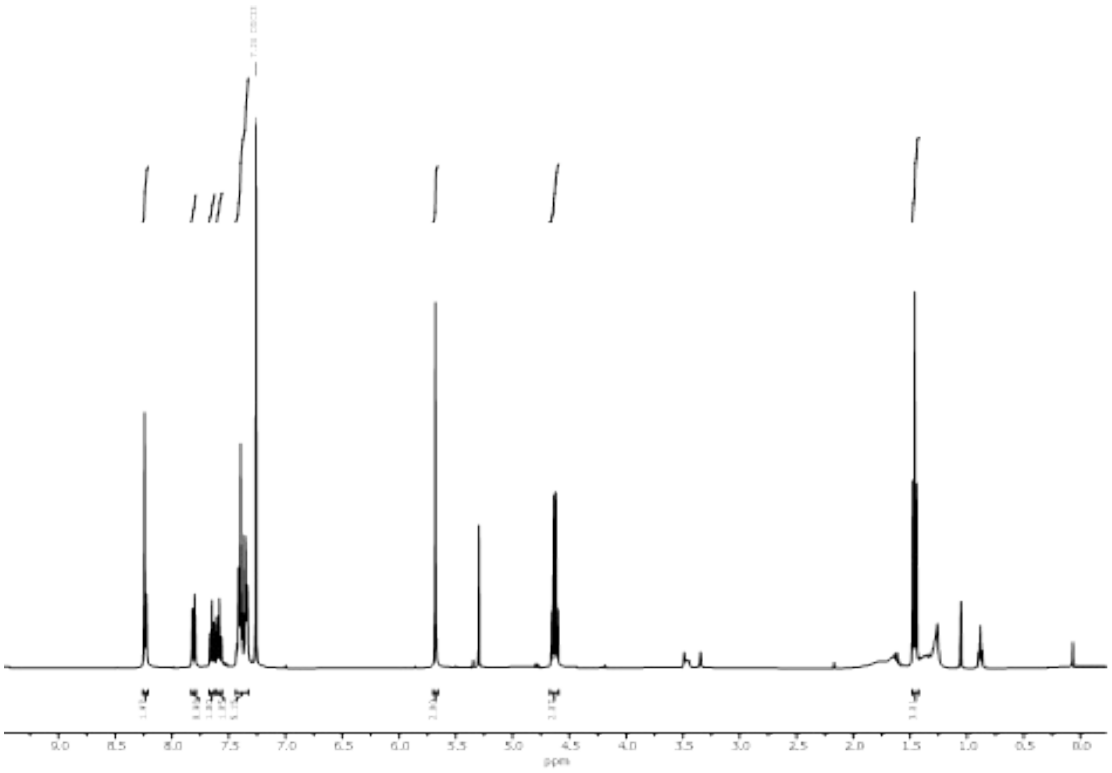

Figure S3. ^{1}H NMR (400 MHz, $CDCl_3$) of ligand **4e (**2-(1-benzyl-1H-1,2,3-triazol-4-yl)-3-ethoxyquinoxaline).

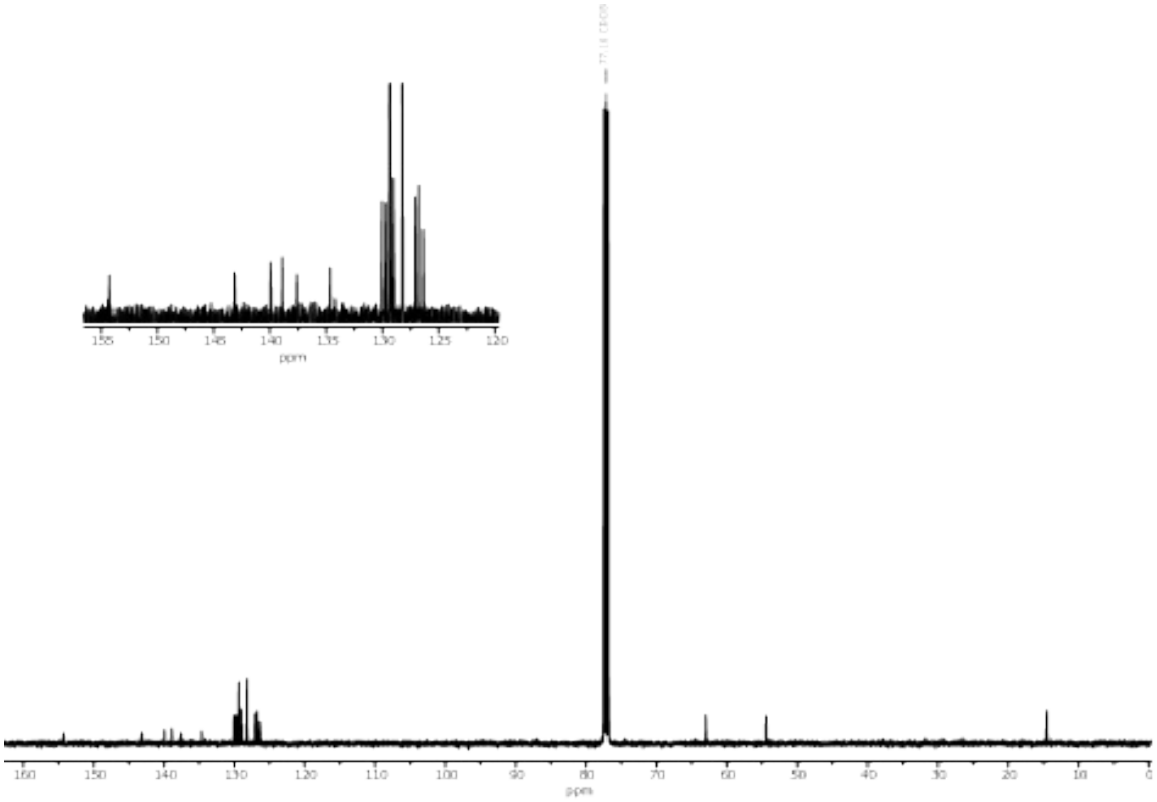

Figure S4. ^{13}C NMR (101 MHz, $CDCl_3$) of ligand **4e, (**2-(1-benzyl-1H-1,2,3-triazol-4-yl)-3-ethoxyquinoxaline).

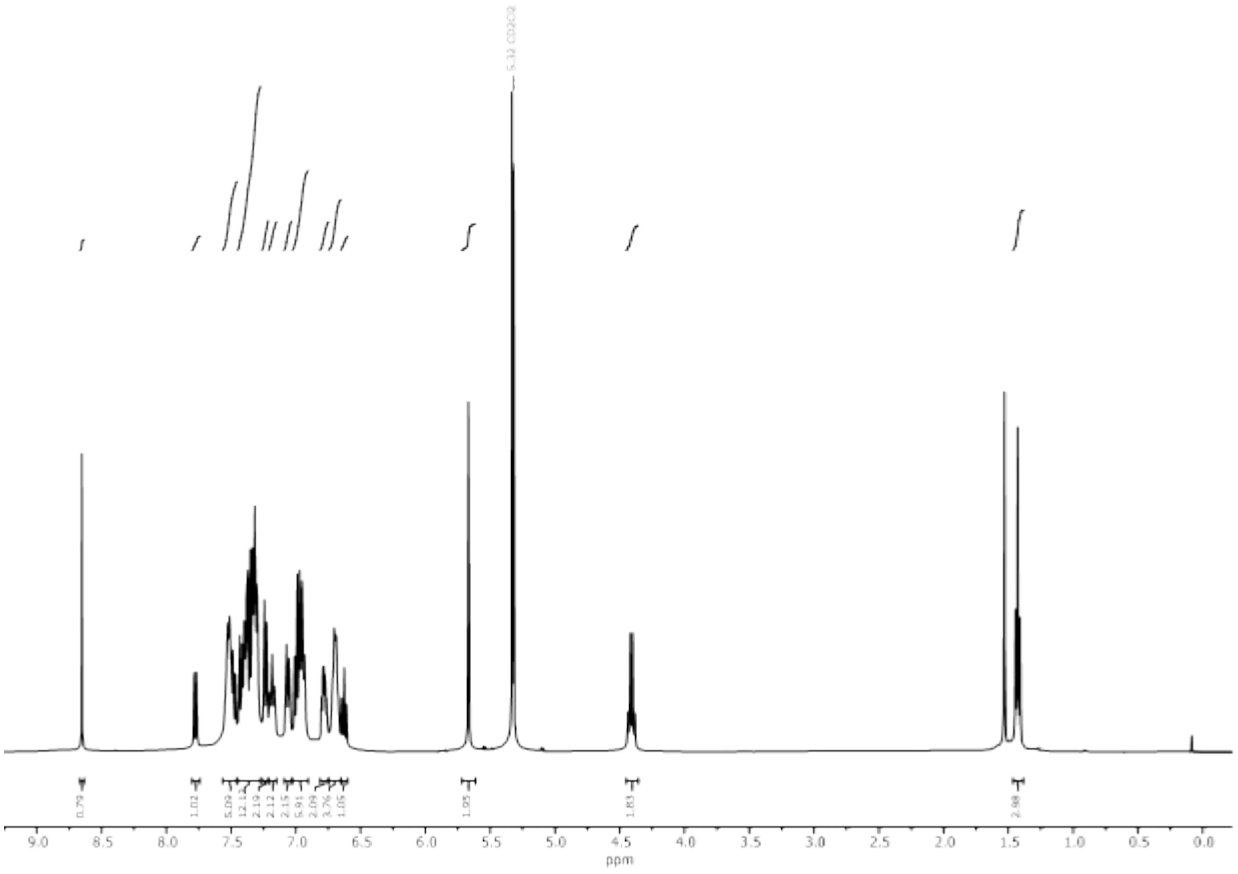

Figure S5. ^{1}H NMR (400 MHz, $CDCl_3$) of Cu(I) complex **5k**.

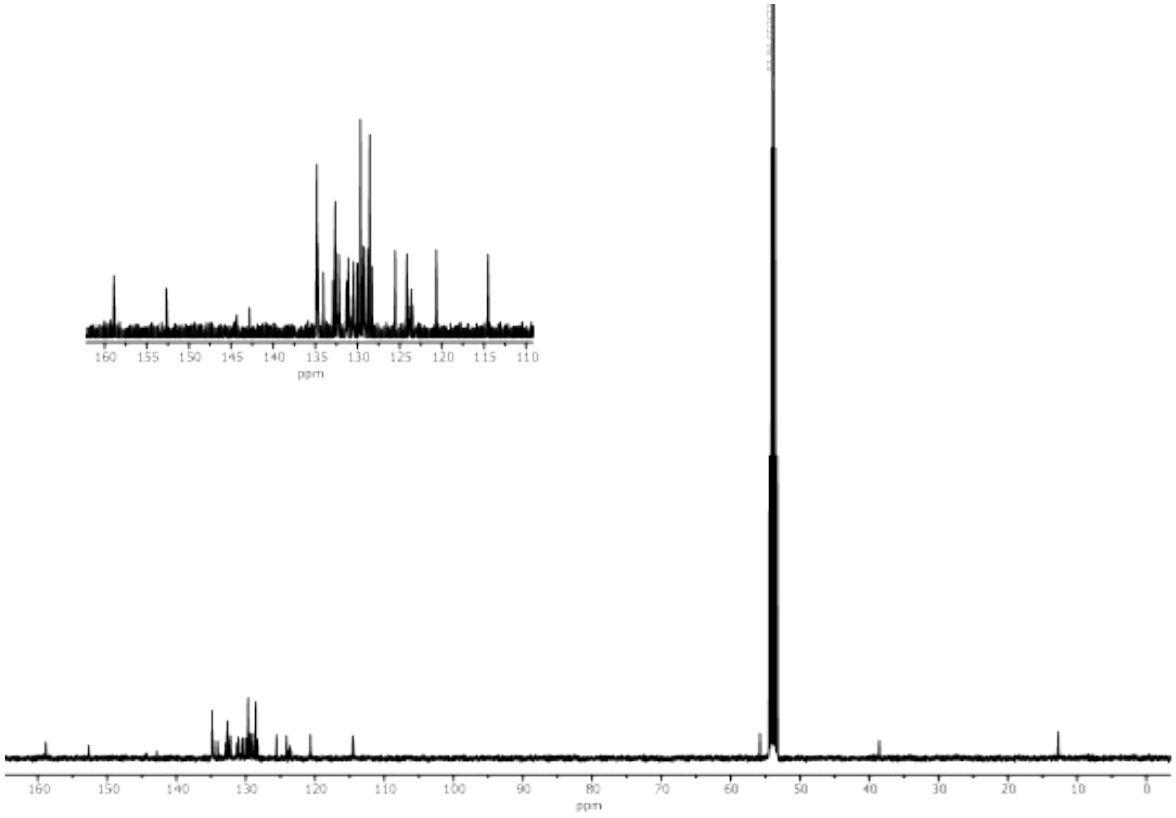

Figure S6. ^{13}C NMR (101 MHz, $CDCl_3$) of Cu(I) complex **5k**.

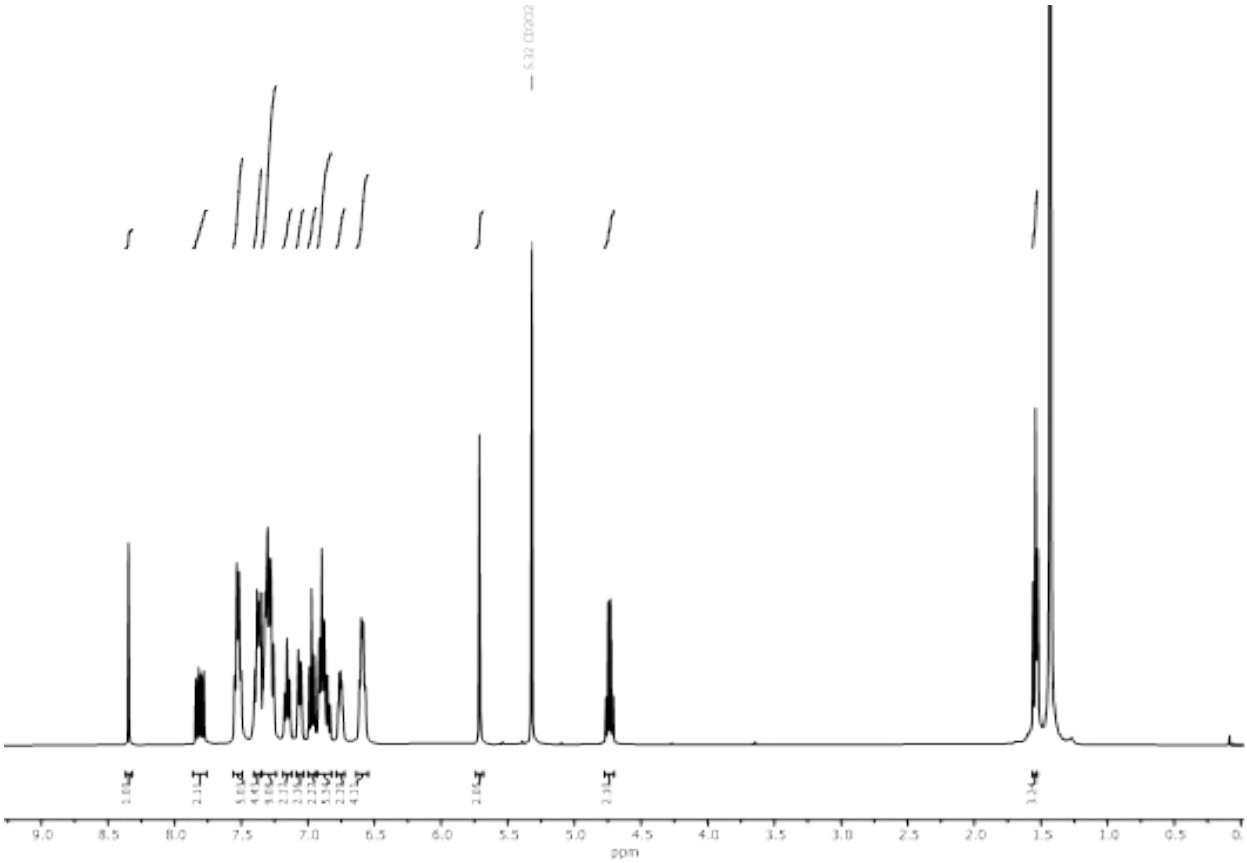

Figure S7. ^{1}H NMR (400 MHz, $CDCl_3$) of Cu(I) complex **5e**.

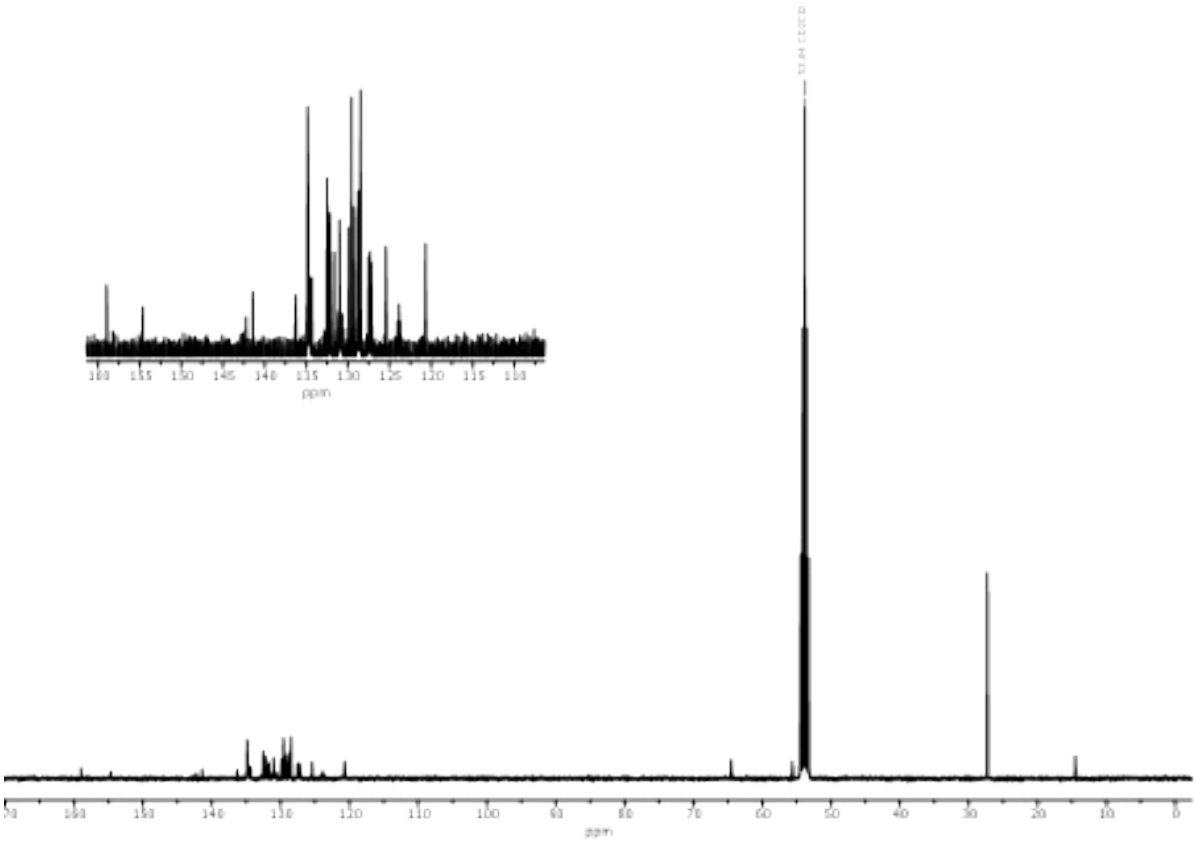

Figure S8. ^{13}C NMR (101 MHz, $CDCl_3$) of Cu(I) complex **5e**.

3. Single crystal X-ray analysis

Single crystal X-ray diffraction data were collected on a Stoe StadiVari diffractometer with monochromated Ga Kα (1.34143 Å) radiation generated by an Excillium MetalJet at low temperature. Using Olex2 [1], the structures were solved with the ShelXT [2] structure solution program using Intrinsic Phasing and refined with the ShelXL [3] refinement package using Least Squares minimization. Refinement was performed with anisotropic temperature factors for all non-hydrogen atoms; hydrogen atoms were calculated on idealized positions. Crystallographic data and refinement details are summarized in Table S1.

Crystallographic data for compounds **3e**, **4e**, **5k** and **5e** reported in this paper have been deposited with the Cambridge Crystallographic Data Centre as supplementary information no. CCDC-2495572–2495575. Copies of the data can be obtained free of charge from https://www.ccdc.cam.ac.uk/structures/.

Table S1. Crystallographic data and refinement details of **3e** and **4e**.

Compound	**3e**	**4e**
Empirical formula	$C_{21}H_{30}N_2OSi$	$C_{19}H_{17}N_5O$
Formula weight	354.56	331.38
Temperature/K	150	150
Crystal system	triclinic	monoclinic
Space group	*P*	$P2_1/c$
a/Å	8.5621(3)	7.9579(2)
b/Å	11.0550(4)	18.3644(7)
c/Å	12.5523(5)	11.2638(3)
α/°	65.642(3)	90
β/°	73.994(3)	93.225(2)
γ/°	74.747(3)	90
Volume/Å^3	1025.16(7)	1643.51(9)
Z	2	4
ρ_{calc}g/cm^3	1.149	1.339
μ/mm^{-1}	0.697	0.451
F(000)	384.0	696.0

Crystal size/mm^3	0.18 × 0.16 × 0.14	0.21 × 0.19 × 0.17
Radiation	GaKα (λ = 1.34143)	GaKα (λ = 1.34143)
2Θ range for data collection/°	6.85 to 127.872	8.02 to 124.962
Index ranges	–11 ≤ h ≤ 6, –14 ≤ k ≤ 14, –16 ≤ l ≤ 16	–3 ≤ h ≤ 10, –24 ≤ k ≤ 24, -–14 ≤ l ≤ 14
Reflections collected	12050	28413
Independent reflections	4913 [R_{int} = 0.0157]	3957 [R_{int} = 0.0257
Indep. refl. with I≥2σ (I)	4443	3293
Data/restraints/parameters	4913/0/233	3957/0/227
Goodness-of-fit on F^2	1.065	1.059
Final R indexes [I≥2σ (I)]	R_1 = 0.0341, wR_2 = 0.0947	R_1 = 0.0342, wR_2 = 0.0883
Final R indexes [all data]	R_1 = 0.0372, wR_2 = 0.0964	R_1 = 0.0429, wR_2 = 0.0918
Largest diff. peak/hole / e Å^{-3}	0.27/–0.32	0.26/–0.23
CCDC number	2495572	2495573

Table S1 (continued). Crystallographic data and refinement details of **5k** and **5e**.

Compound	**5k**	**5e**
Empirical formula	$C_{56}H_{47}Cl_2CuF_6N_5O_2P_3$	$C_{58}H_{51}Cl_6CuF_6N_5O_2P_3$
Formula weight	1163.33	1333.19
Temperature/K	150	180
Crystal system	monoclinic	triclinic
Space group	$P2_1/c$	P
a/Å	10.9697(2)	14.1830(3)
b/Å	30.9030(8)	14.4936(3)
c/Å	15.7518(4)	17.2084(4)
α/°	90	71.464(2)
β/°	94.550(2)	83.167(2)

γ/°	90	63.560(2)
Volume/Å^3	5323.0(2)	3002.03(13)
Z	4	2
ρ_{calc}g/cm^3	1.452	1.475
μ/mm^{-1}	3.759	4.419
F(000)	2384.0	1360.0
Crystal size/mm^3	0.18 × 0.1 × 0.02	0.3 × 0.28 × 0.26
Radiation	GaKα (λ = 1.34143)	GaKα (λ = 1.34143)
2Θ range for data collection/°	5.492 to 124.98	4.714 to 128.362
Index ranges	–14 ≤ h ≤ 5, –40 ≤ k ≤ 39, –20 ≤ l ≤ 20	–18 ≤ h ≤ 18, –18 ≤ k ≤ 19, –7 ≤ l ≤ 22
Reflections collected	33930	36294
Independent reflections	12502 [R_{int} = 0.0254]	14466 [R_{int} = 0.0309]
Indep. refl. with I≥2σ (I)	9511	11122
Data/restraints/parameters	12502/0/677	14466/0/734
Goodness-of-fit on F^2	1.092	1.037
Final R indexes [I≥2σ (I)]	R_1 = 0.0554, wR_2 = 0.1431	R_1 = 0.0913, wR_2 = 0.2627
Final R indexes [all data]	R_1 = 0.0773, wR_2 = 0.1526	R_1 = 0.1107, wR_2 = 0.2858
Largest diff. peak/hole / e Å^{-3}	1.55/–1.51	1.00/–1.37
CCDC number	2495574	2495575

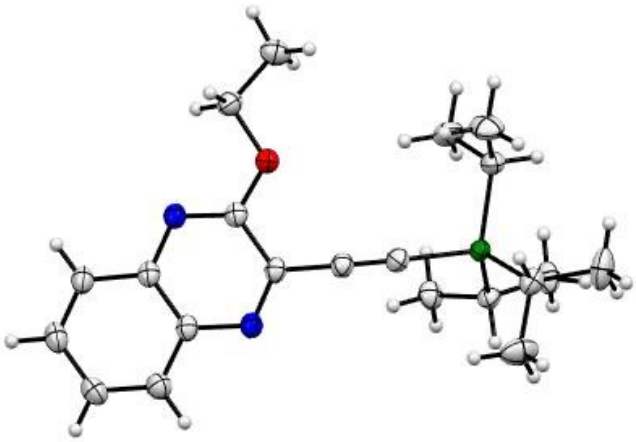

Figure S9. ORTEP drawing of crystal 2-ethoxy-3-((triisopropylsilyl)ethynyl)quinoxaline **(3e)**.

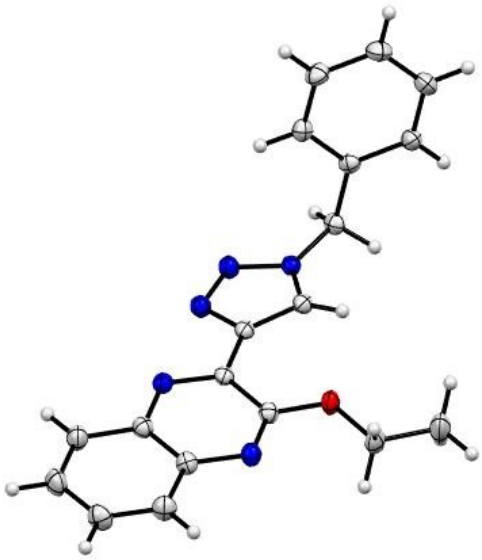

Figure S10. ORTEP drawing of crystal 2-(1'-benzyl-1'H-1',2',3'-triazol-4'-yl)-3-ethoxyquinoxaline **(4e)**.

4. Stability tests of the complexes

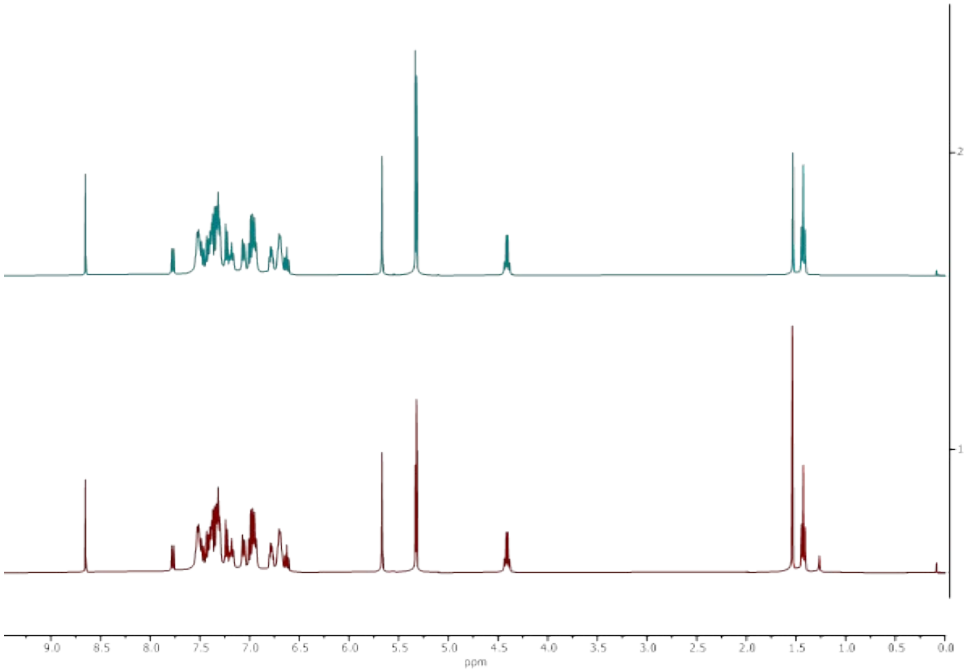

Figure S11. ^{1}H NMR (400 MHz) of **5k** in CD_2Cl_2: freshly prepared solution (top) and after a week (bottom).

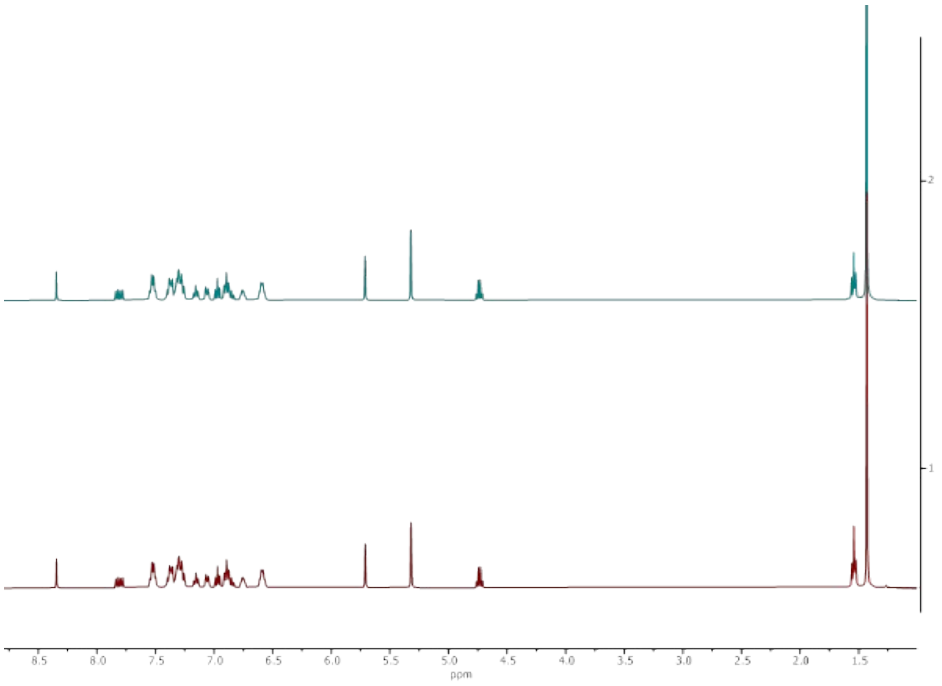

Figure S12. ^{1}H NMR (400 MHz) of **5e** in CD_2Cl_2: freshly prepared solution (top) and after a week (bottom).

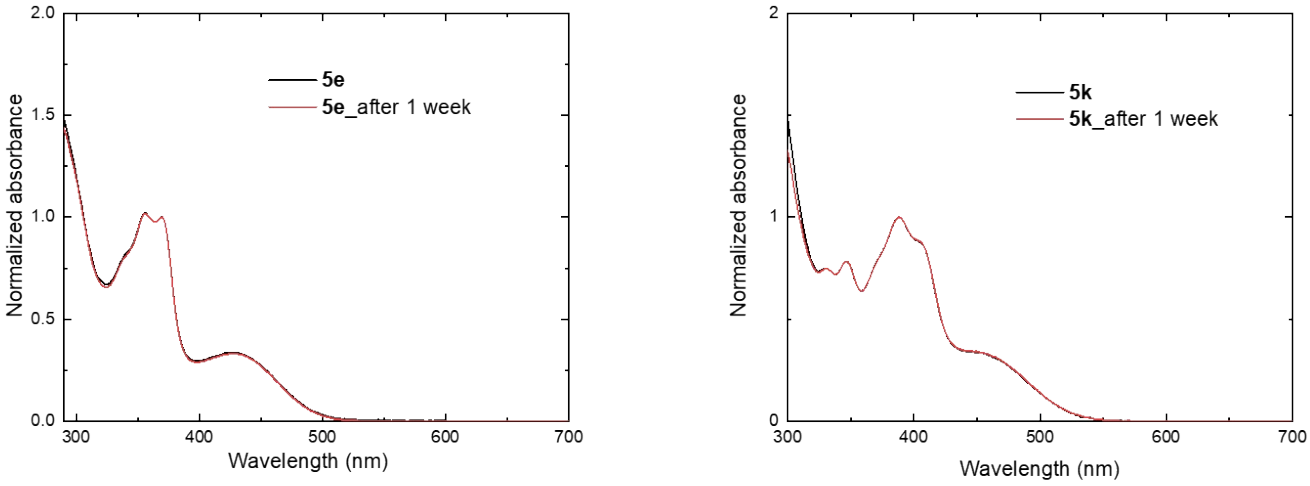

Figure S13. UV-vis absorption spectra of a solution of **5e** (left) and **5k** (right), freshly prepared (black curve) and after one week (red curve).

5. Additional photophysical data

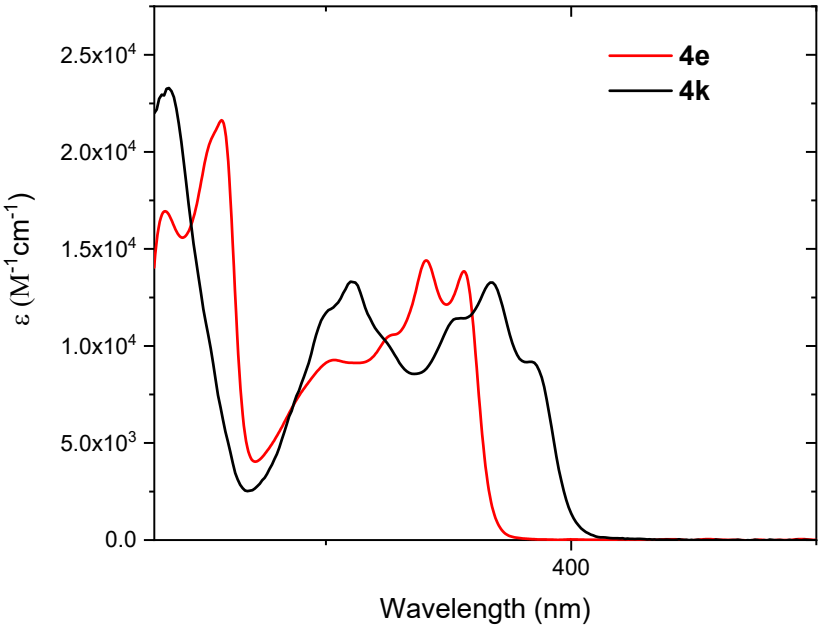

Figure S14. UV-vis absorption spectra of the ligands **4e** (red curve) and **4k** (black curve) in dichloromethane.

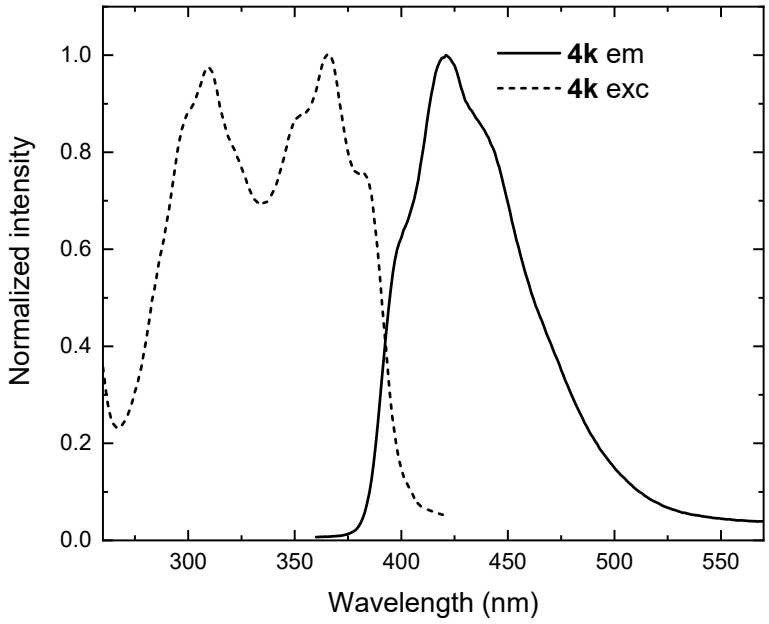

Figure S15. Excitation (dotted line) and emission (solid line) spectra of the ligand **4k** in dichloromethane.

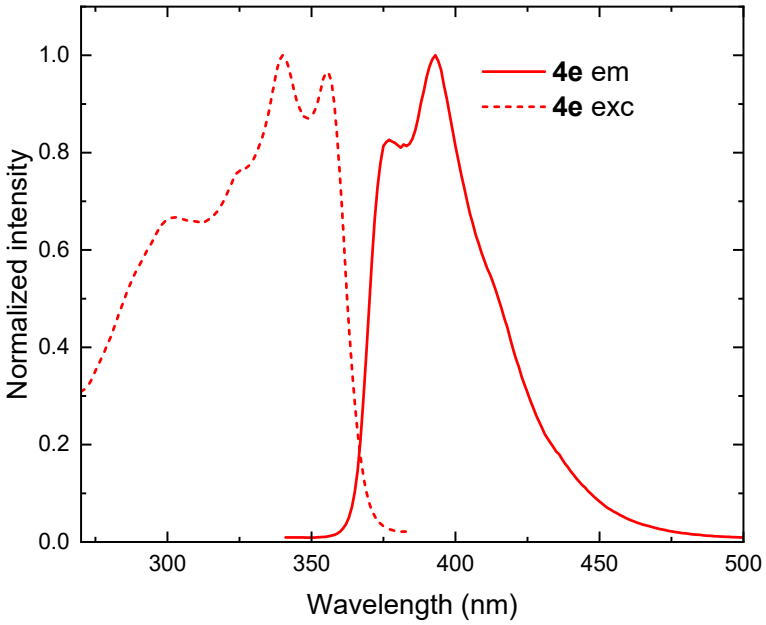

Figure S16. Excitation (dotted line) and emission (solid line) spectra of the ligand **4e** in dichloromethane.

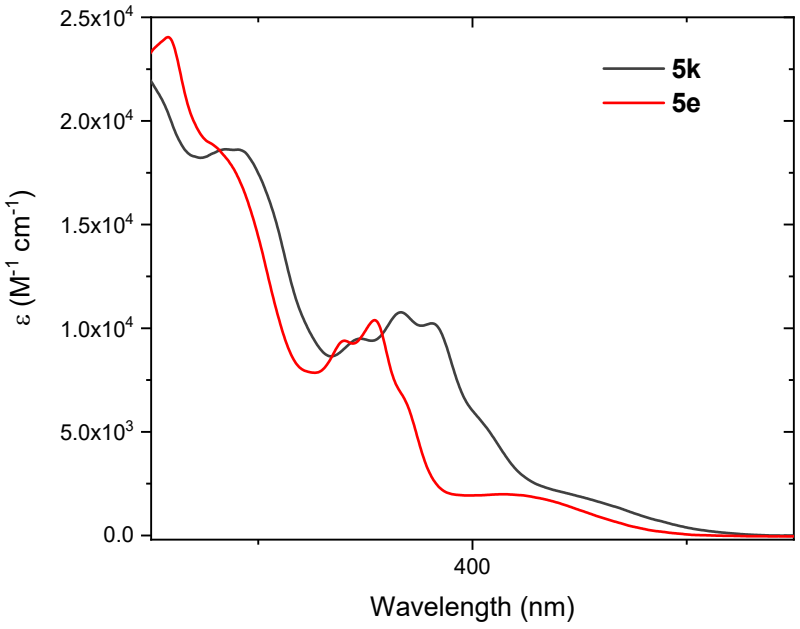

Figure S17. Absorption spectra of the Cu(I) complexes **5e** (red curve) and **5k** (black curve) in acetonitrile.

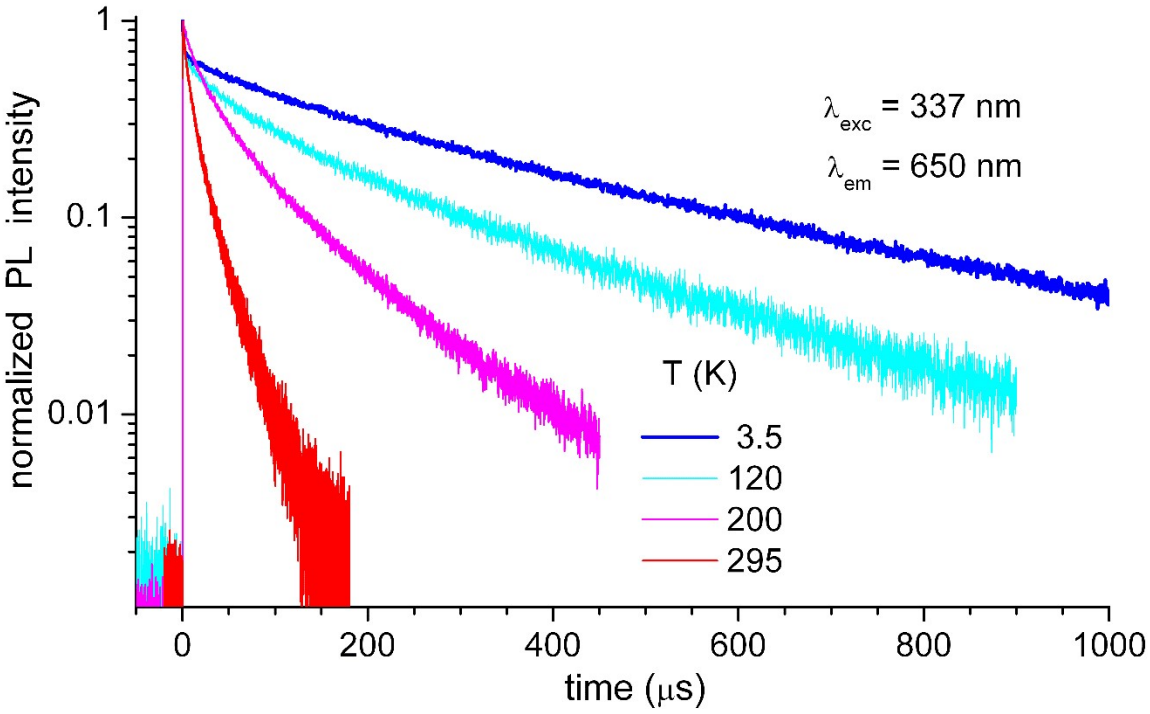

Figure S18. PL decay versus temperature of Cu(I) complex **5e**.

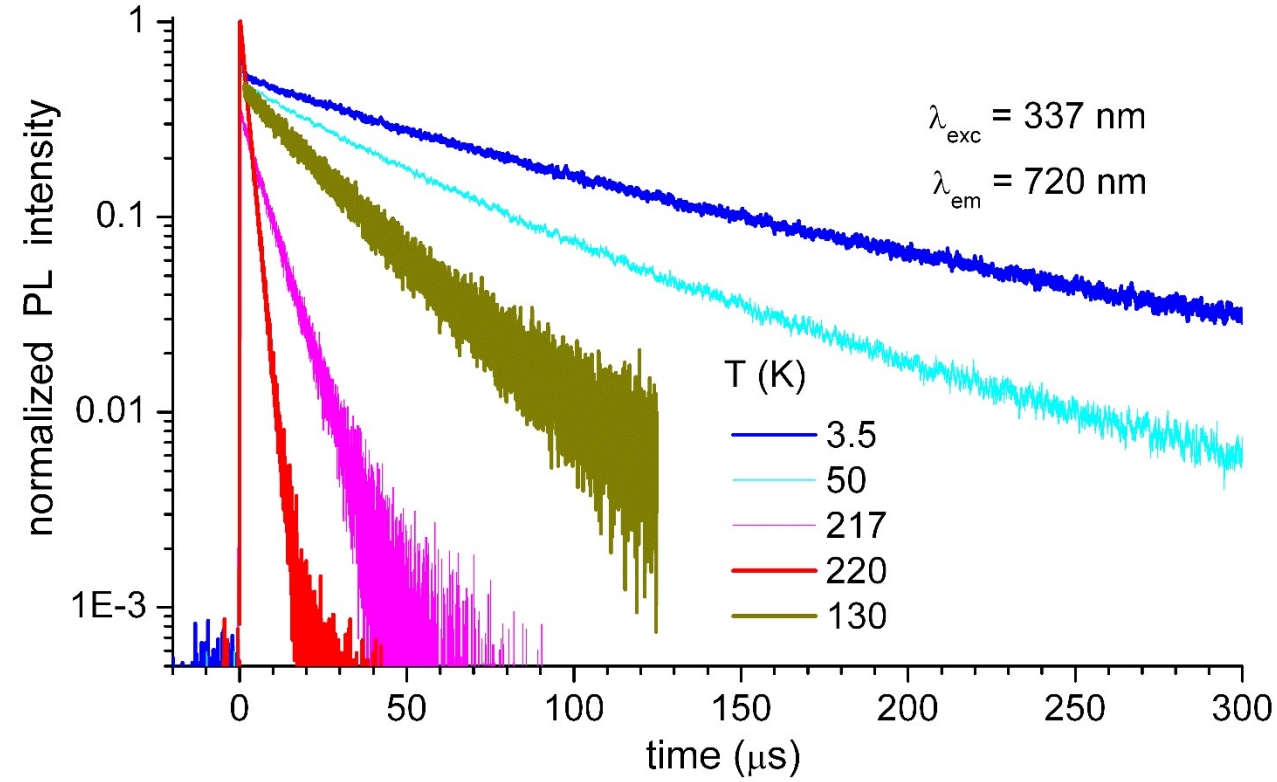

Figure S19. PL decay versus temperature of Cu(I) complex **5k**.

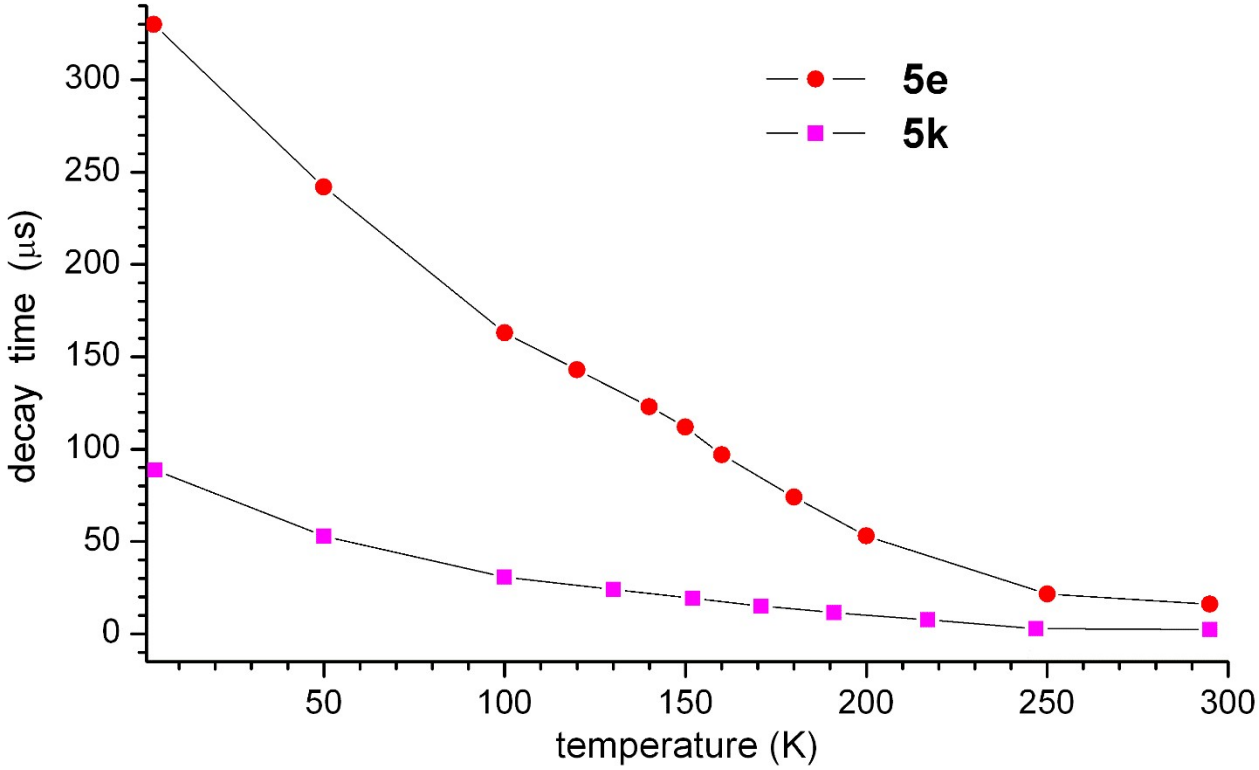

Figure S20. Decay time versus temperature of Cu(I) complexes **5k** (pink squares) and **5e (**red dots).

6. Additional quantum-chemical data

Table S2. Excitation energies and oscillator strengths of the five lowest singlet excitations of ligands **4k** and **4e**. The excitation with the largest oscillator strength, S_2, is a transition from the highest occupied molecular orbital (HOMO, H) to the lowest unoccupied molecular orbital (LUMO, L). The smaller excitation energy of **4k** compared to **4e** is connected to a smaller HOMO-LUMO gap, where the HOMO is shifted to higher energies and the LUMO is shifted to lower energies.

4k				**4e**			
	E (eV)	f	Dominant contribution		E (eV)	f	Dominant contribution
S_1	3.85	0.007		S_1	4.01	0.001	
S_2	4.00	0.505	91.1% H → L	S_2	4.27	0.437	78.0% H → L
S_3	4.59	0.207		S_3	4.62	0.140	
S_4	5.22	0.002		S_4	5.47	0.002	
S_5	5.52	0.050		S_5	5.53	0.000	

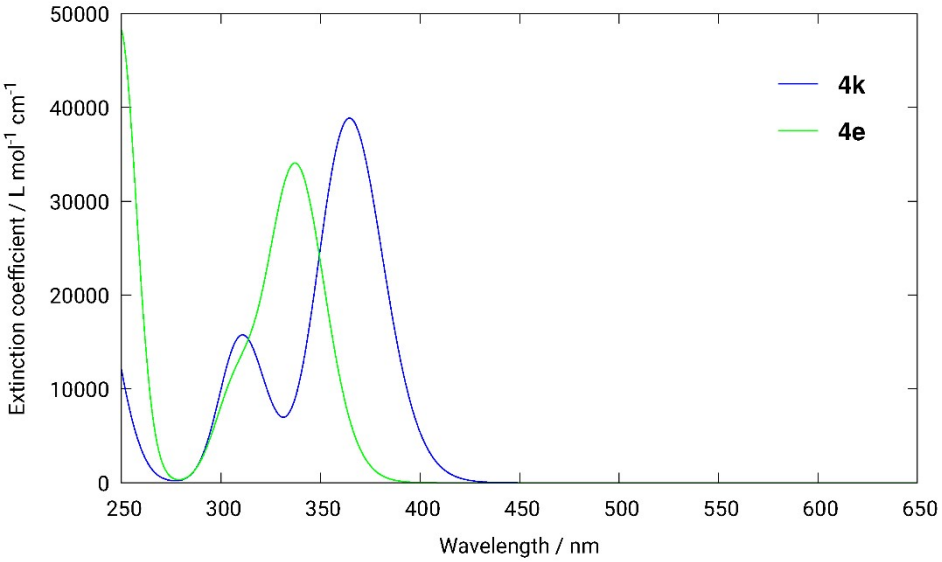

Figure S21. Simulated absorption spectra of **4k** and **4e**. For better comparison with experiment, the computed line spectra were broadened with Gaussian-shape functions (rms line width: 0.15 eV) and shifted to lower energies (by −0.6 eV).

Table S3. Excitation energies and oscillator strengths of the five lowest singlet excitations of **5k** and **5e**. The lowest excitation, S_1, is a transition from the highest occupied molecular orbital (HOMO, H) to the lowest unoccupied molecular orbital (LUMO, L). This excitation corresponds to a metal-to-ligand charge transfer from Cu to the keto-amine or enol-imine ligand (^{1}MLCT state). The smaller excitation energy of **5k** compared to **5e** can be explained by the observation that the LUMO is shifted to lower energies in the corresponding ligand **4k**.

5k				**5e**			
	E (eV)	f	Dominant contribution		E (eV)	f	Dominant contribution
S_1	3.46	0.074	90.2% H → L	S_1	3.61	0.072	91.1% H → L
S_2	3.69	0.208		S_2	3.87	0.003	
S_3	3.72	0.042		S_3	4.02	0.225	
S_4	4.05	0.006		S_4	4.20	0.019	
S_5	4.31	0.117		S_5	4.28	0.069	

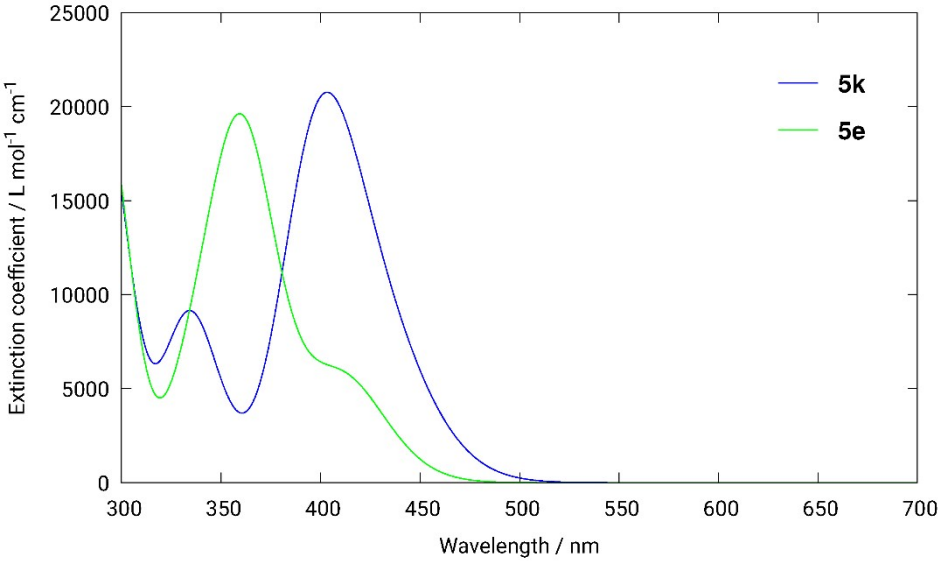

Figure S22. Simulated absorption spectra of **5k** and **5e**. For better comparison with experiment, the computed line spectra were broadened with Gaussian-shape functions (rms line width: 0.15 eV) and shifted to lower energies (by −0.6 eV).

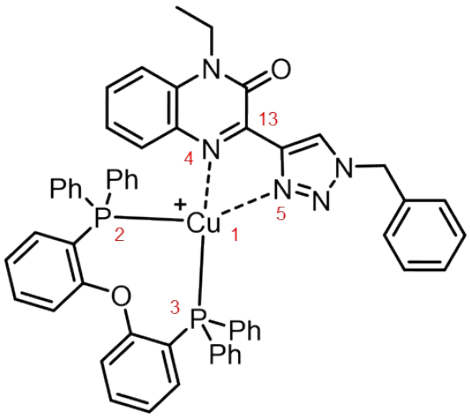

5k

Table S4. Selected bond lengths and bond angles for the computed S_0, ^{1}MLCT and ^{3}MLCT geometries and comparison with the x-ray structure.

5k	1–2 (Å)	1–3 (Å)	1–4 (Å)	1–5 (Å)	2–1–3 (°)	4–1–5 (°)
X-ray	2.244	2.232	2.085	2.066	112.5	79.6
S_0	2.312	2.295	2.165	2.106	116.3	78.1
^{1}MLCT	2.346	2.413	2.043	2.072	106.4	82.1
^{3}MLCT	2.342	2.360	1.981	2.083	106.1	82.3

Table S5. Change of selected bond lengths and bond angles for the computed S_0, ^{1}MLCT and ^{3}MLCT geometries.

5k	1–2 (pm)	1–3 (pm)	1–4 (pm)	1–5 (pm)	4–13 (pm)	2–1–3 (°)	4–1–5 (°)
$S_0 \rightarrow {}^1$MLCT	+3.5	+11.8	−12.2	−3.4	+5.6	−9.9	+4.0
$S_0 \rightarrow {}^3$MLCT	+3.0	+6.6	−18.4	−2.3	+7.4	−10.2	+4.2
^{1}MLCT $\rightarrow {}^3$MLCT	−0.4	−5.3	−6.2	+1.2	+1.7	−0.3	+0.2

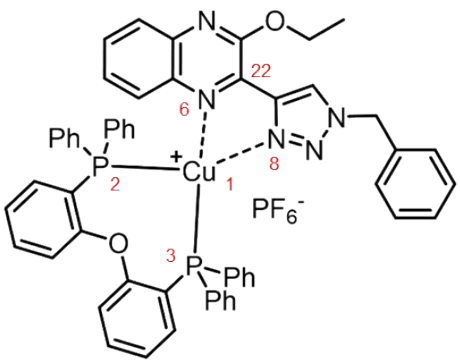

5e

Table S6. Selected bond lengths and bond angles for the computed S_0, ^{1}MLCT and ^{3}MLCT geometries and comparison with the x-ray structure.

5e	1–2 (Å)	1–3 (Å)	1–6 (Å)	1–8 (Å)	2–1–3 (°)	6–1–8 (°)
X-ray	2.250	2.243	2.122	2.048	111.1	79.7
S_0	2.296	2.312	2.152	2.108	116.2	78.1
^{1}MLCT	2.365	2.418	2.048	2.048	104.2	81.7
^{3}MLCT	2.362	2.378	1.984	2.052	104.9	81.9

Table S7. Change of selected bond lengths and bond angles for the computed S_0, ^{1}MLCT and ^{3}MLCT geometries.

5e	1–2 (pm)	1–3 (pm)	1–6 (pm)	1–8 (pm)	6–22 (pm)	2–1–3 (°)	6–1–8 (°)
$S_0 \rightarrow {}^1$MLCT	+7.0	+10.6	−10.5	−6.0	+5.4	−12.1	+3.6
$S_0 \rightarrow {}^3$MLCT	+6.6	+6.6	−16.8	−5.7	+6.4	−11.4	+3.8
^{1}MLCT $\rightarrow {}^3$MLCT	−0.3	−4.0	−6.3	+0.3	+1.0	−0.7	−0.2

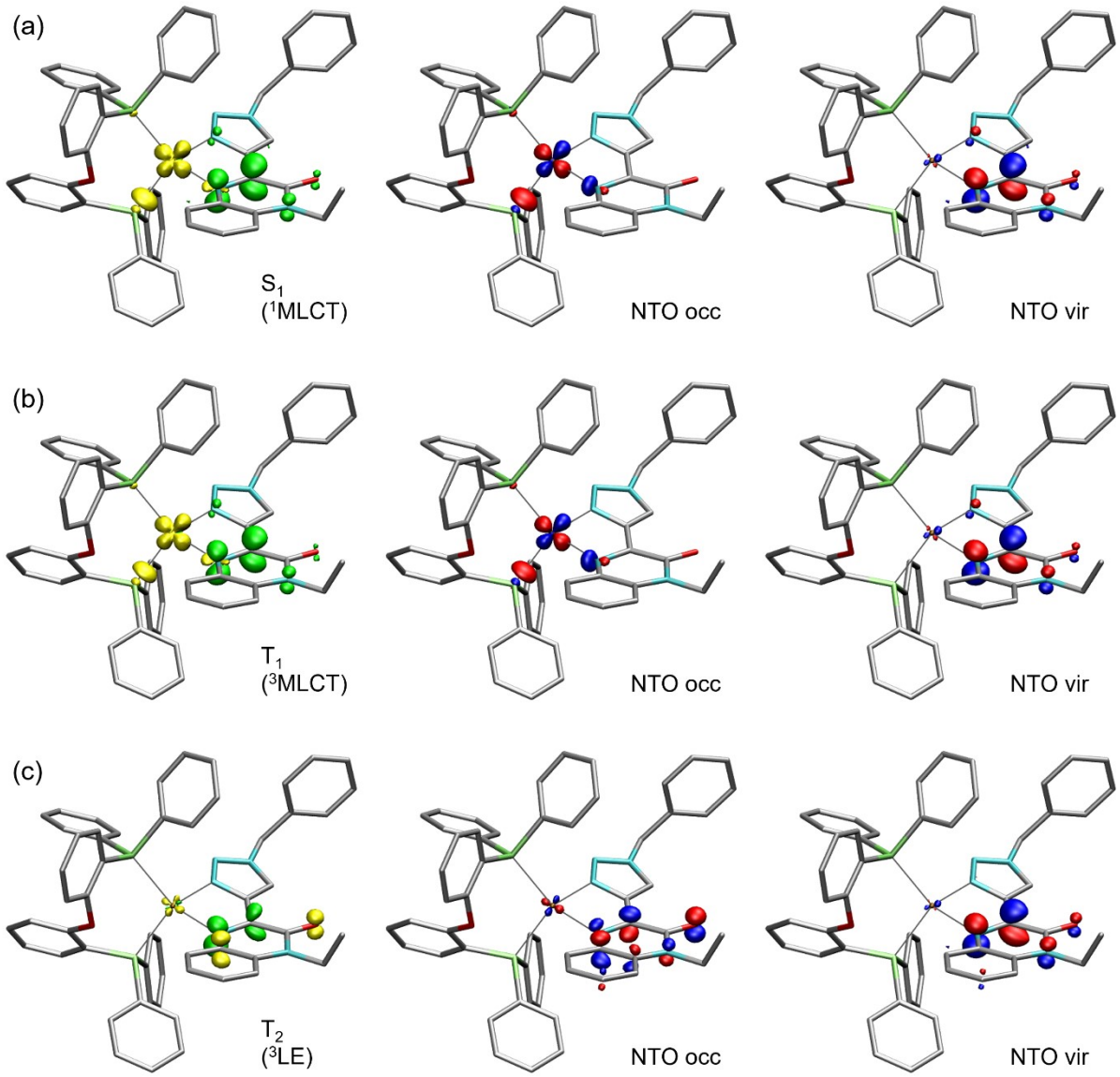

Figure S23. Difference between the electron density of the ground state and the excited states (a) S_1, (b) T_1 and (c) T_2 of complex **5k** at the optimized ^{1}MLCT geometry ((isovalue ±0.01 bohr^{-3}). Electron density is transferred from yellow to green regions. The corresponding pair of natural transition orbitals that describes the electron (NTO occ) and the hole (NTO vir) is also given (isovalue ±0.1 bohr$^{-3/2}$). Hydrogen atoms are omitted for clarity.

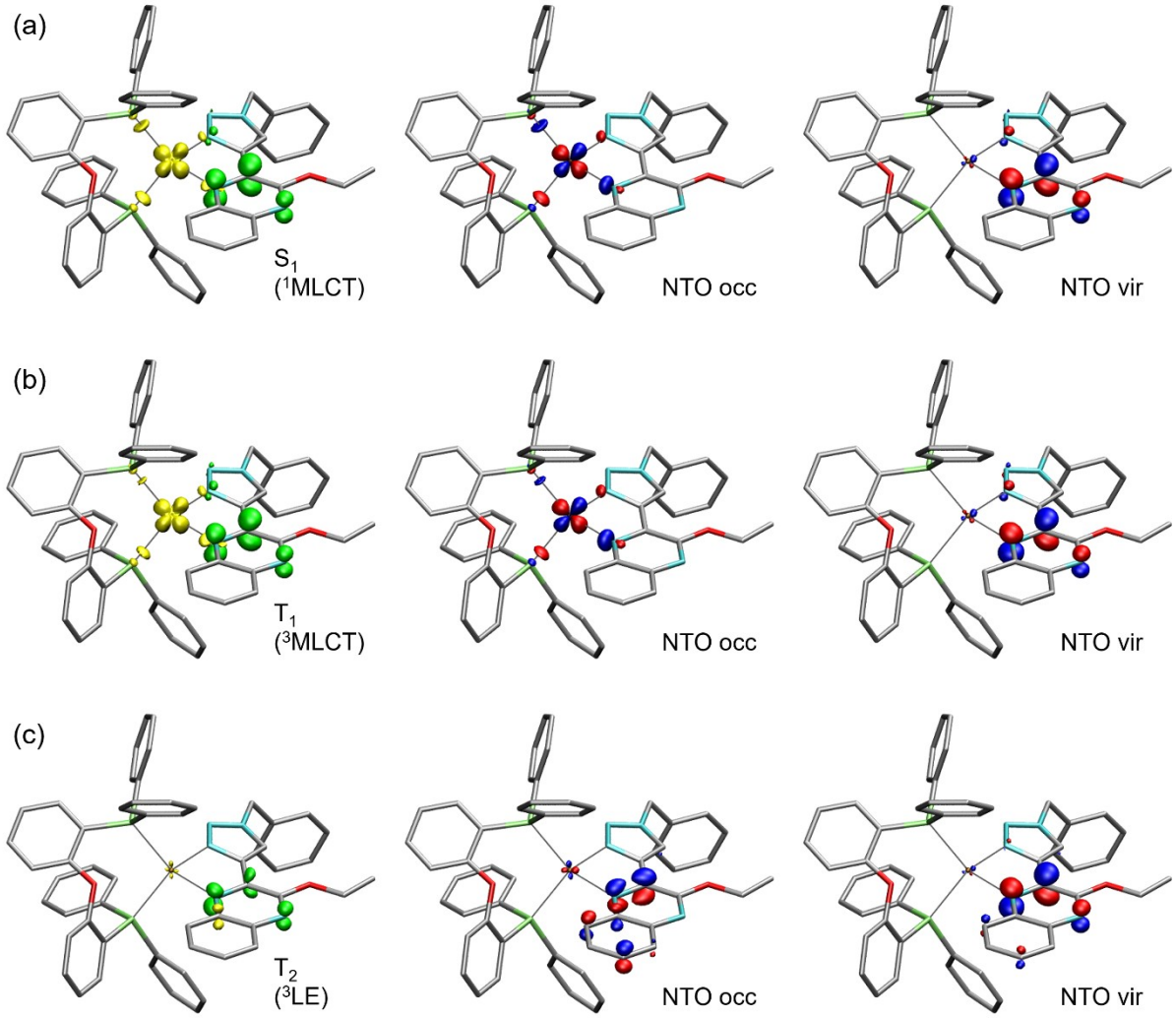

Figure S24. Difference between the electron density of the ground state and the excited states (a) S_1, (b) T_1 and (c) T_2 of complex **5e** at the optimized ^{1}MLCT geometry ((isovalue ±0.01 bohr^{-3}). Electron density is transferred from yellow to green regions. The corresponding pair of natural transition orbitals that describes the electron (NTO occ) and the hole (NTO vir) is also given (isovalue ±0.1 bohr$^{-3/2}$). Hydrogen atoms are omitted for clarity.

Table S8. Values of the quantity Λ used to measure the degree of spatial overlap between the pair of natural transition orbitals that describes the electron (NTO occ) and the hole (NTO vir) involved in the respective excitation.

5k			**5e**		
	S_0 geometry	^{1}MLCT geometry		S_0 geometry	^{1}MLCT geometry
S_1	0.32	0.36	S_1	0.35	0.35
T_1	–	0.47	T_1	–	0.39
T_2	–	0.82	T_2	–	0.85

Table S9. Estimated singlet-triplet energy gaps for the CT states using different approximations. All values are given in eV.

	5k	**5e**
$\Delta E(S_1-T_1)@S_0$	0.21	0.10
$\Delta E(S_1-T_1)@S_1$	0.15	0.14
$\Delta E(S_1-T_1)@T_1$	0.41	0.28
$E(S_1)@S_1-E(T_1)@T_1$	0.37	0.26
ΔE exp	0.11	0.05

7. Electrochemical data of the ligands

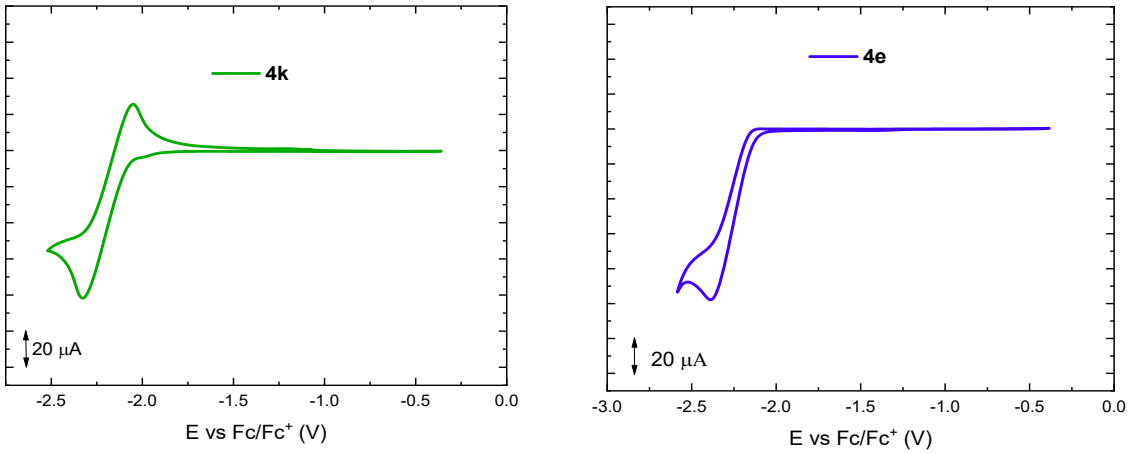

Figure S25. Cyclic voltammetry of the ligands **4k** (left, green curve) and **4e** (right, blue curve) in a 0.1M $TBAPF_6$ solution in dichloromethane. Scan rate 100 mV/s.

8. Additional photocurrent measurements

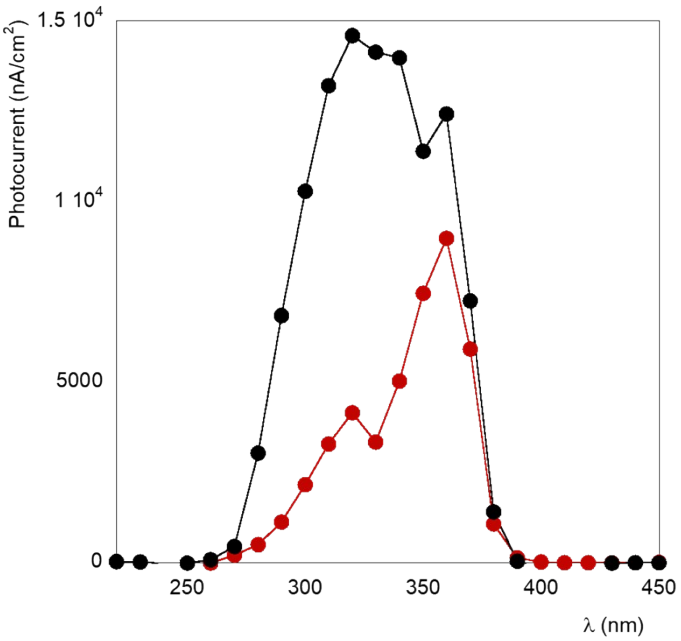

Figure S26. Photocurrent action spectra of film **5k** (black) and **5e** (red) on TiO_2/FTO electrodes. The measurements have been performed in aqueous TEOA solution, at 0 V (vs. Ag/AgCl), upon photoirradiation at different wavelengths (every 10 nm from 200 to 600 nm).

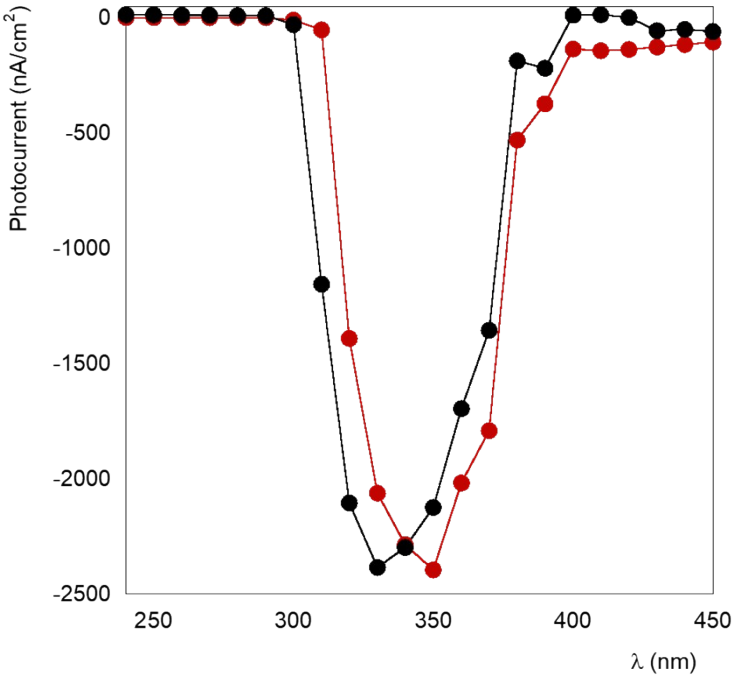

Figure S27. Photocurrent action spectra of film **5k** (black) and **5e** (red) on TiO_2/FTO electrodes. The measurements have been performed in aqueous methylviologen solution, at 0 V (vs. Ag/AgCl), upon photoirradiation at different wavelengths (every 10 nm from 200 to 600 nm).

9. References

[1] O.V. Dolomanov, L.J. Bourhis, R.J. Gildea, J.A.K. Howard, H. Puschmann, *J. Appl. Cryst.* **2009**, *42*, 339–341.

[2] G.M. Sheldrick, *Acta Cryst. A* **2015**, *A71*, 3–8.

[3] G.M. Sheldrick, *Acta Cryst. C* **2015**, *C71*, 3–8.